05

Synthesis, structural, resonant and magnetic properties $NaMnFe_2(VO_4)_3$

© T.V. Drokina, M.S. Molokeev, O.A. Bayukov, D.A. Velikanov, A.M. Vorotynov, G.A. Petrakovsky

Kirensky Institute of Physics, Federal Research Center KSC SB, Russian Academy of Sciences, Krasnoyarsk, Russia

¶ E-mail: tvd@iph.krasn.ru

Received April 19, 2024
Revised April 19, 2024
Accepted April 24, 2024

The compound $NaMnFe_2(VO_4)_3$ was obtained by solid-phase synthesis from the starting oxides Na_2CO_3, Fe_2O_3, $MnCO_3$ and V_2O_5. The structural and static magnetic properties were studied, and the material was characterized using Mössbauer spectroscopy and electron paramagnetic resonance.

The parameters of the trigonal unit cell (space group $P1$) were determined and the crystal structure was refined (the coordinates of the atoms and their isotropic thermal parameters, the main lengths of interatomic bonds are given). The structural features of $NaMnFe_2(VO_4)_3$ allow for the existence of competing magnetic exchange interactions, as well as the formation of a state of local violation of charge neutrality.

The chain magnetic subsystem $NaMnFe_2(VO_4)_3$, formed by Mn^{2+} and iron Fe^{3+} cations, in the temperature range $T > 50$ K is characterized primarily by antiferromagnetic exchange interaction and the molar value of the effective magnetic moment $\mu_{eff(ex)} = 9.9\,\mu_B$. At temperatures below 10.5 K, the temperature dependence of the magnetic moment depends on the thermal history of the sample.

Keywords: inorganic compounds, multicomponent vanadates, crystal structure, resonant and magnetic properties.

DOI: 10.61011/PSS.2024.08.59053.94

1. Introduction

The development of new materials (in particular, vanadium-based oxide compounds containing magnetic cations [1–4]) is an integral part of modern condensed matter physics. Multicomponent vanadates with general chemical formula $AMeFe_2V_3O_{12}$ (A denotes monovalent alkaline earths and Me stands for bivalent metals) are among these materials. The interest in them stems from their physical properties that are related directly to crystallographic features.

The crystal structure of $LiCuFe_2(VO_4)_3$ and $NaCuFe_2(VO_4)_3$ vanadates is characterized by triclinic space group P-1 [3,5,6]. Chemical pressure resulting from the substitution of lithium with sodium in the $ACuFe_2(VO_4)_3$ system induces an anisotropic change in the crystal lattice parameters without violating its symmetry [6]. The magnetism of $LiCuFe_2(VO_4)_3$ is typically characterized by antiferromagnetic exchange interaction and a high level of frustration in the chain spin structure [3]. The parameters of exchange interactions in the six-sublattice representation of $LiCuFe_2(VO_4)_3$ were estimated within indirect coupling model. It was demonstrated that the compound is an antiferromagnetic with strong intrachain and frustrating interchain exchange interactions [3]. It follows from the results of studies into the magnetism in $NaCuFe_2(VO_4)_3$ that antiferromagnetism and (at lower temperatures) spin disorder are observed in howardevansite [4,6]. The evaluation of parameters of exchange interactions in $NaCuFe_2(VO_4)_3$ revealed the presence of strong intrachain and weak interchain exchange interactions [4].

The crystal structure of $NaNiFe_2(VO_4)_3$ is characterized by triclinic space group $P1$ [7], which differs from space group P-1 typical of copper-containing compounds $LiCuFe_2(VO_4)_3$ and $NaCuFe_2(VO_4)_3$. In addition to paramagnetism, temperature and field dependences of the sample magnetization reveal ferromagnetic properties in the high-temperature region; at low temperatures, disordered magnetism is observed [7,8].

The crystal structure of $NaZnFe_2(VO_4)_3$ is characterized by triclinic space group $P1$. The chain magnetic subsystem, which is characterized by a negative asymptotic Néel temperature, undergoes a magnetic transition from the paramagnetic state to the magnetic spin glass state [9] when the temperature decreases.

The study of multicomponent vanadates with general chemical formula $AMeFe_2V_3O_{12}$ ($A = \mathrm{Li, Na}$; $Me = \mathrm{Ni, Cu, Zn}$) demonstrated that the specific feature of their crystal structures is the dispersal of metal cations over crystallographically non-equivalent mixed sites with uneven filling with cations of iron Fe^{3+} and bivalent metal. Thus, the crystal structures of the examined compounds allow for competing exchange interactions and the formation of various types of magnetic ordering shaped by a complex configuration of magnetic interactions.

Note that the physical properties of vanadates of the $AMeFe_2V_3O_{12}$ system were examined for a small number of materials. Therefore, the synthesis and investigation of new multicomponent vanadates remain relevant. In the present study, we report the results of synthesis and evaluation of characteristics of $NaMnFe_2V_3O_{12}$, which is a new member of the group of multicomponent vanadates.

2. Sample synthesis and experimental procedure

$NaMnFe_2V_3O_{12}$ samples were produced by solid-phase synthesis from a stoichiometric mixture of high-purity oxides Na_2CO_3, Fe_2O_3, $MnCO_3$, V_2O_5:

$$1/2Na_2CO_3 + Fe_2O_3 + MnCO_3 + 3/2V_2O_5 \rightarrow NaMnFe_2V_3O_{12}.$$

The initial compounds constituting the charge were dried at a temperature of 105°C for six hours before weighing. The stoichiometric mixture containing Na_2CO_3 (2.4 wt.%), Fe_2O_3 (22.0 wt.%), $MnCO_3$ (11.4 wt.%), and V_2O_5 (64.2 wt.%) was ground with the addition of ethyl alcohol. Tablets were formed from the prepared charge under a pressure of approximately 10 kbar and annealed in a furnace. The first annealing was carried out at a temperature of 600° for 24 hours in air. After that, the tablets were ground, re-formed, and subjected to a second annealing at a temperature of 650°C for 24 hours in air. The chemical and phase composition of the synthesized samples was monitored via X-ray diffraction analysis.

The powder X-ray diffraction pattern of $NaMnFe_2V_3O_{12}$ was recorded at room temperature with a Bruker D8 ADVANCE diffractometer, a VANTEC linear detector, and Cu-Kα radiation. Different primary beam slit sizes were used in the experiment: 0.6 mm — at angles $2\theta = 5°-70°$; 2 mm — in the 70°–120° range. The scan step was 0.016° and remained constant in all region; the exposure time at each step was 2.7 and 1.8 s within the 5°–70° and 70°–120° ranges, respectively. Standard deviations of intensities of all points of the X-ray pattern were then calculated, and the intensities and the standard deviations of all points of the large-angle part were multiplied by a normalizing coefficient of 0.6.

The static magnetic properties of $NaMnFe_2V_3O_{12}$ were studied with a SQUID magnetometer of an original design at the Kirensky Institute of Physics [10,11] within the 4–300 K temperature range in two modes: zero-field cooling (ZFC) and field cooling (FC).

The electron magnetic resonance spectra of $NaMnFe_2V_3O_{12}$ were measured using a Bruker Elexsys E580 spectrometer in the X band within the 110–300 K temperature range. The following parameters were set to record the spectra: microwave power, 0.63 mW; modulation amplitude, 0.7 G; modulation frequency, 100 kHz; magnetic field sweep width, 5 kG; sweep time, 40 s.

Nuclear gamma resonance spectra were recorded with an MS-1104Em spectrometer at the Kirensky Institute of Physics at room temperature with a $Co^{57}(Rh)$ source for powders with a thickness of 5–10 mg/cm^2 in natural iron content. The chemical shifts are indicated relative to α-Fe.

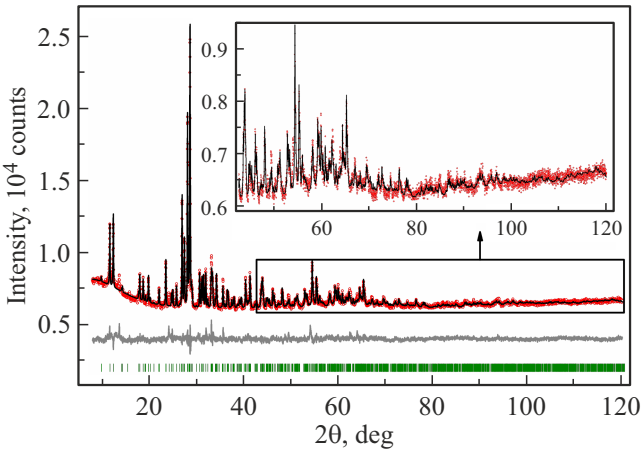

Figure 1. Differential X-ray diffraction pattern of $NaMnFe_2(VO_4)_3$.

3. Experimental results and discussion

3.1. Results of structural studies of $NaMnFe_2(VO_4)_3$

Figure 1 presents the powder X-ray diffraction pattern of the $NaMnFe_2V_3O_{12}$ compound at room temperature. Experimental and calculated X-ray profiles after refinement by the Rietveld method are shown at the top. The next curve is the differential X-ray diffraction pattern. Line marks at the bottom of figure denote the calculated positions of reflections.

Almost all reflections are characterized by a triclinic cell with parameters close to those of $NaFe_3(VO_4)_3$ [12]; therefore, this structure was used as the initial one. Since the refinement of Fe/Mn occupancy was extremely unstable due to the proximity of atomic scattering functions, all six Fe ion sites were populated with Fe/Mn ions with fixed site occupancies according to chemical formula Fe/Mn = 2 : 1. Coordinates of Na1 were not refined, which is needed to fix the origin in polar group $P1$. Rietveld refinement was implemented in TOPAS 4.2 [13]. The results of refinement are presented in Table 1 and Figure 1. The atomic coordinates and thermal parameters are listed in Table 2, and the main bond lengths in the structure of multicomponent iron and manganese vanadate are indicated in Table 3.

The crystal structure of the $NaMnFe_2(VO_4)_3$ compound is shown in Figure 2.

According to X-ray diffraction data, multicomponent vanadate $NaMnFe_2(VO_4)_3$ crystallizes in a triclinic structure

Table 1. Key parameters of the X-ray experiment and results of crystal structure refinement for $NaMnFe_2V_3O_{12}$ at temperature $T = 300$ K

Parameter	Value
Sp. gr.	$P1$
a, Å	6.7624 (2)
b, Å	8.2444 (3)
c, Å	9.8570 (3)
α, °	105.935 (2)
β, °	104.761 (3)
γ, °	102.761 (3)
V, Å^3	487.38 (3)
Interval 2θ, °	5–120
Number of reflections	1473
Number of refined param.	160
R_{wp}, %	1.77
R_p, %	1.35
R_B, %	0.96
χ^2	1.66

Note. a, b, c, α, β, and γ are the lattice cell parameters; V is the cell volume; interval 2θ is the measurement interval; unreliability factors: R_{wp} — weight profile, R_p — profile, R_B — integral; and χ^2 is the quality of fit.

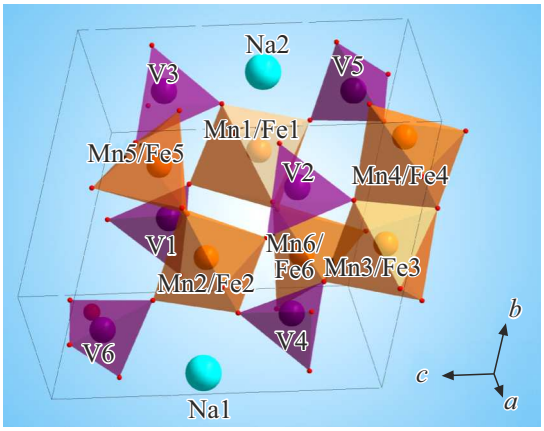

Figure 2. Crystal structure of $NaMnFe_2(VO_4)_3$.

with two molecules in a lattice cell, and its symmetry is characterized by space group $P1$. Six mixed non-equivalent crystallographic Fe_i/Mn_i ($i = 1–6$) sites are present in the structure of iron-manganese vanadate. Four of them have an octahedral oxygen environment, and two have an anionic environment in the form of a trigonal bipyramid. The $(Fe_i^{3+}/Mn_i^{2+})O_j$ ($j = 5, 6$) formations are linked by common vertices into endless chains $(\ldots -(Fe^{3+}1/Mn^{2+}1)-(Fe^{3+}2/Mn^{2+}2)-(Fe^{3+}5/Mn^{2+}5)-(Fe^{3+}4/Mn^{2+}4)-(Fe^{3+}3/Mn^{2+}3)-(Fe^{3+}6/Mn^{2+}6)\ldots)$, extending in the **a**–**c** direction. The chains are connected to each other by tetrahedral anionic complexes $(VO_4)^{3-}$, forming a two-dimensional layer in a plane based on two vectors **a**–**c** and **b**. The layers are bound by VO_4 into a three-dimensional structure. The channels of the structure are filled with Na^+ cations, which occupy two non-equivalent crystallographic sites.

The charge composition of the compound has the following form: $Na^+Mn^{2+}Fe_2^{3+}(V^{5+}O_4^{2-})_3$. Local violation of charge neutrality (Table 2) is observed due to the mixing of iron cations Fe^{3+} with Mn^{2+} cations in the lattice cell of vanadate at the same crystal site.

Figure 3 and Table 4 present the results of room-temperature Mössbauer studies of iron-manganese vanadate.

A model spectrum consisting of two doublets was plotted based on the data retrieved from distribution P(QS) of quadrupolar splittings in the experimental spectrum. The model spectrum was fitted to the experimental one by varying all hyperfine structure parameters.

The results of Mössbauer spectroscopy provided an opportunity to examine the state of iron in vanadate $NaMnFe_2V_3O_{12}$. It was found that all iron cations in the compound are in high-spin state $3d^5$ with spin $S = 5/2$ and occupy two types of crystal sites differing in oxygen environment: chemical shift $IS = 0.39$ mm/s relative to α-Fe and quadrupolar splitting $QS = 0.52$ mm/s correspond to the sites of iron cations in an octahedral oxygen environment, while $IS = 0.33$ mm/s and $QS = 1.08$ mm/s correspond to Fe^{3+} cations in a bipyramidal oxygen environment.

Thus, a lattice cell of the crystal structure of $NaMnFe_2V_3O_{12}$ contains six mixed sites occupied by Fe^{3+} and Mn^{2+} cations: four of them are octahedral, and the other two are bipyramidal. The occupancy of octahedral sites by iron cations is approximately three times higher than that of bipyramidal sites. The Mössbauer data are indicative of a preferential distribution of Fe^{3+} cations in the crystal lattice of the $NaMnFe_2V_3O_{12}$ compound over octahedral sites.

3.2. Results of EPR studies of $NaMnFe_2V_3O_{12}$

Figure 4 shows the EPR spectrum of $NaMnFe_2V_3O_{12}$ recorded at a frequency of 9 GHz and temperatures $T = 302.8$ K, 261.9 K, and 222.3 K (a) and the results of fitting of the experimental EPR spectrum at $T = 302.8$ K with two Lorentzian absorption curves *1* and *2* (b). The solid curve corresponds to the experimental data, while the dotted curve is the result of fitting (Figure 4, b).

Figure 5 shows the temperature dependences of intensity I (a), resonance field H_{res} (b), and line width dH (c) for fitting curves *1* and *2*. Intensity was determined as the area under the EPR fitting curves.

At $T = 302.8$ K, the Landé g-factor values for curves *1* and *2* are $g_1 = 2.012$ and $g_2 = 2.673$, respectively.

It follows from the analysis of EPR data that signal *1* is produced by the main $NaMnFe_2V_3O_{12}$ matrix. The intensity of this signal is two orders of magnitude higher than the one of signal *2*. Curve *2* is probably associated with the formation of a small amount of hematite superparamagnetic particles upon the Implantation of bivalent manganese cations in the process of synthesis. The estimated amount of this supplementary phase does not exceed 4%. This

Table 2. Atomic coordinates, isotropic thermal parameters B_{iso}, and site occupancy (Occ.) in the crystal structure of $NaMnFe_2(VO_4)_3$ at temperature $T = 300$ K

Atom	x	y	z	B_{iso}, Å^2	Occ.
Na1	0.99425	0.07762	0.5534	2 (2)	1
Na2	0.475 (16)	1.004 (12)	0.488 (12)	1 (1)	1
Fe1	0.108 (10)	0.564 (7)	0.384 (6)	0.4 (3)	0.667
Mn1	0.108 (10)	0.564 (7)	0.384 (6)	0.4 (3)	0.333
Fe2	0.877 (10)	0.467 (8)	0.604 (6)	0.4 (3)	0.667
Mn2	0.877 (10)	0.467 (8)	0.604 (6)	0.4 (3)	0.333
Fe3	0.462 (10)	0.333 (7)	0.993 (7)	0.4 (3)	0.667
Mn3	0.462 (10)	0.333 (7)	0.993 (7)	0.4 (3)	0.333
Fe4	0.547 (10)	0.767 (7)	0.024 (6)	0.4 (3)	0.667
Mn4	0.547 (10)	0.767 (7)	0.024 (6)	0.4 (3)	0.333
Fe5	0.795 (9)	0.790 (8)	0.797 (7)	0.4 (3)	0.667
Mn5	0.795 (9)	0.790 (8)	0.797 (7)	0.4 (3)	0.333
Fe6	0.222 (10)	0.211 (8)	0.202 (7)	0.4 (3)	0.667
Mn6	0.222 (10)	0.211 (8)	0.202 (7)	0.4 (3)	0.333
V1	0.403 (11)	0.435 (9)	0.663 (7)	0.7 (3)	1
V2	0.598 (11)	0.612 (8)	0.326 (7)	0.7 (3)	1
V3	0.273 (9)	0.866 (7)	0.743 (7)	0.7 (3)	1
V4	0.723 (11)	0.185 (8)	0.278 (8)	0.7 (3)	1
V5	0.087 (10)	0.769 (7)	0.132 (7)	0.7 (3)	1
V6	0.905 (10)	0.219 (8)	0.876 (7)	0.7 (3)	1
O1	0.43 (2)	0.448 (15)	0.854 (15)	0.9 (5)	1
O2	0.58 (2)	0.547 (16)	0.141 (16)	0.9 (5)	1
O3	0.379 (18)	0.474 (14)	0.353 (15)	0.9 (5)	1
O4	0.63 (2)	0.537 (15)	0.649 (17)	0.9 (5)	1
O5	0.25 (2)	0.802 (14)	0.554 (15)	0.9 (5)	1
O6	0.76 (2)	0.207 (15)	0.448 (16)	0.9 (5)	1
O7	0.51 (2)	0.216 (15)	0.164 (15)	0.9 (5)	1
O8	0.50 (2)	0.763 (16)	0.833 (14)	0.9 (5)	1
O9	0.15 (2)	0.262 (15)	0.009 (16)	0.9 (5)	1
O10	0.84 (2)	0.729 (14)	0.994 (15)	0.9 (5)	1
O11	0.18 (2)	0.474 (15)	0.586 (15)	0.9 (5)	1
O12	0.82 (2)	0.514 (17)	0.424 15)	0.9 (5)	1
O13	0.02 (2)	0.713 (16)	0.737 (16)	0.9 (5)	1
O14	0.97 (2)	0.286 (15)	0.262 (15)	0.9 (5)	1
O15	0.32 (2)	0.058 (14)	0.819 (16)	0.9 (5)	1
O16	0.68 (2)	0.948 (15)	0.177 (16)	0.9 (5)	1
O17	0.34 (2)	0.195 (14)	0.579 (14)	0.9 (5)	1
O18	0.65 (2)	0.801 (15)	0.420 (15)	0.9 (5)	1
O19	0.20 (2)	0.000 (16)	0.237 (14)	0.9 (5)	1
O20	0.81 (2)	0.999 (17)	0.775 (15)	0.9 (5)	1
O21	0.28 (2)	0.726 (13)	0.052 (13)	0.9 (5)	1
O22	0.75 (2)	0.273 (15)	0.968 (16)	0.9 (5)	1
O23	0.07 (2)	0.655 (16)	0.241 (15)	0.9 (5)	1
O24	0.93 (2)	0.332 (14)	0.746 (16)	0.9 (5)	1

Table 3. Main bond lengths in the crystal structure of $NaMnFe_2(VO_4)_3$ at $T = 300$ K

Bond	Length, Å	Bond	Length, Å
Na1–O5^{i}	3.15 (8)	Mn4–O1^{vii}	2.53 (11)
Na1–O6	2.29 (9)	Mn4–O2	2.42 (10)
Na1–O11^{ii}	3.14 (7)	Mn4–O8^{vii}	1.81 (13)
Na1–O15^{ii}	3.03 (12)	Mn4–O10^{vii}	2.12 (9)
Na1–O17^{ii}	2.27 (8)	Mn4–O16	1.68 (13)
Na1–O18^{iii}	2.62 (9)	Mn4–O21	1.86 (9)
Na1–O20^{iii}	2.94 (11)	Fe5–O4	2.06 (12)
Na1–O24	2.62 (11)	Fe5–O8	2.10 (9)
Na2–O5	2.34 (10)	Fe5–O10	2.10 (13)
Na2–O6^{iv}	2.45 (10)	Fe5–O13^{ii}	1.92 (10)
Na2–O17^{iv}	2.07 (11)	Fe5–O20	1.79 (10)
Na2–O18	2.31 (11)	Mn5–O4	2.06 (12)
Na2–O19^{iv}	2.67 (15)	Mn5–O8	2.10 (9)
Na2–O20	3.15 (15)	Mn5–O10	2.10 (13)
Fe1–O3	2.18 (7)	Mn5–O13^{ii}	1.92 (10)
Fe1–O5	2.04 (12)	Mn5–O20	1.79 (10)
Fe1–O11	2.29 (13)	Fe6–O3	2.12 (11)
Fe1–O12^{v}	2.05 (10)	Fe6–O7	2.04 (9)
Fe1–O14^{v}	2.14 (10)	Fe6–O9	2.02 (14)
Fe1–O23	1.75 (12)	Fe6–O14^{v}	2.08 (10)
Mn1–O3	2.18 (7)	Fe6–O19	1.85 (9)
Mn1–O5	2.04 (12)	Mn6–O3	2.12 (11)
Mn1–O11	2.29 (13)	Mn6–O7	2.04 (9)
Mn1–O12^{v}	2.05 (10)	Mn6–O9	2.02 (14)
Mn1–O14^{v}	2.14 (10)	Mn6–O14^{v}	2.08 (10)
Mn1–O23	1.75 (12)	Mn6–O19	1.85 (9)
Fe2–O4	2.00 (9)	V1–O1	1.82 (14)
Fe2–O6	2.11 (12)	V1–O3	3.12 (14)
Fe2–O11^{ii}	2.10 (9)	V1–O4	1.63 (9)
Fe2–O12	1.88 (13)	V1–O8	2.60 (11)
Fe2–O13^{ii}	1.96 (12)	V1–O11	1.64 (11)
Fe2–O24	2.02 (11)	V1–O17	1.83 (9)
Mn2–O4	2.00 (9)	V2–O2	1.71 (15)
Mn2–O6	2.11 (12)	V2–O3	1.79 (8)
Mn2–O11^{ii}	2.10 (9)	V2–O7	3.06 (10)
Mn2–O12	1.88 (13)	V2–O12	2.02 (11)
Mn2–O13^{ii}	1.96 (12)	V2–O18	1.49 (11)
Mn2–O24	2.02 (11)	V3–O5	1.75 (14)
Fe3–O1	1.87 (11)	V3–O8	2.02 (10)
Fe3–O2^{vi}	1.81 (13)	V3–O11	3.02 (10)
Fe3–O7^{vi}	2.15 (12)	V3–O13	1.89 (9)
Fe3–O9^{vi}	2.13 (10)	V3–O15^{iv}	1.48 (10)
Fe3–O15	2.26 (12)	V4–O6	1.58 (15)
Fe3–O22	2.13 (8)	V4–O7	1.72 (11)
Mn3–O1	1.87 (11)	V4–O12	2.55 (11)
Mn3–O2^{vi}	1.81 (13)	V4–O14	1.79 (10)
Mn3–O7^{vi}	2.15 (12)	V4–O16^{iii}	1.85 (10)
Mn3–O9^{vi}	2.13 (10)	V5–O10^{viii}	1.78 (12)
Mn3–O15	2.26 (12)	V5–O19^{iv}	1.78 (11)
Mn3–O22	2.13 (8)	V5–O21	1.75 (10)
Fe4–O1^{vii}	2.53 (11)	V5–O23	1.62 (11)
Fe4–O2	2.42 (10)	V6–O9^{ix}	1.72 (13)
Fe4–O8^{vii}	1.81 (13)	V6–O20^{iii}	1.70 (11)
Fe4–O10^{vii}	2.12 (9)	V6–O22	1.64 (10)
Fe4–O16	1.68 (13)	V6–O24	1.79 (11)
Fe4–O21	1.86 (9)		

Note. Symmetry elements: (i) $x + 1, y, z$; (ii) $x, y - 1, z$; (iii) $x, y + 1, z$; (iv) $x - 1, y, z$; (v) $x, y, z + 1$; (vi) $x, y, z - 1$; (vii) $x - 1, y, z - 1$; (viii) $x + 1, y, z + 1$.

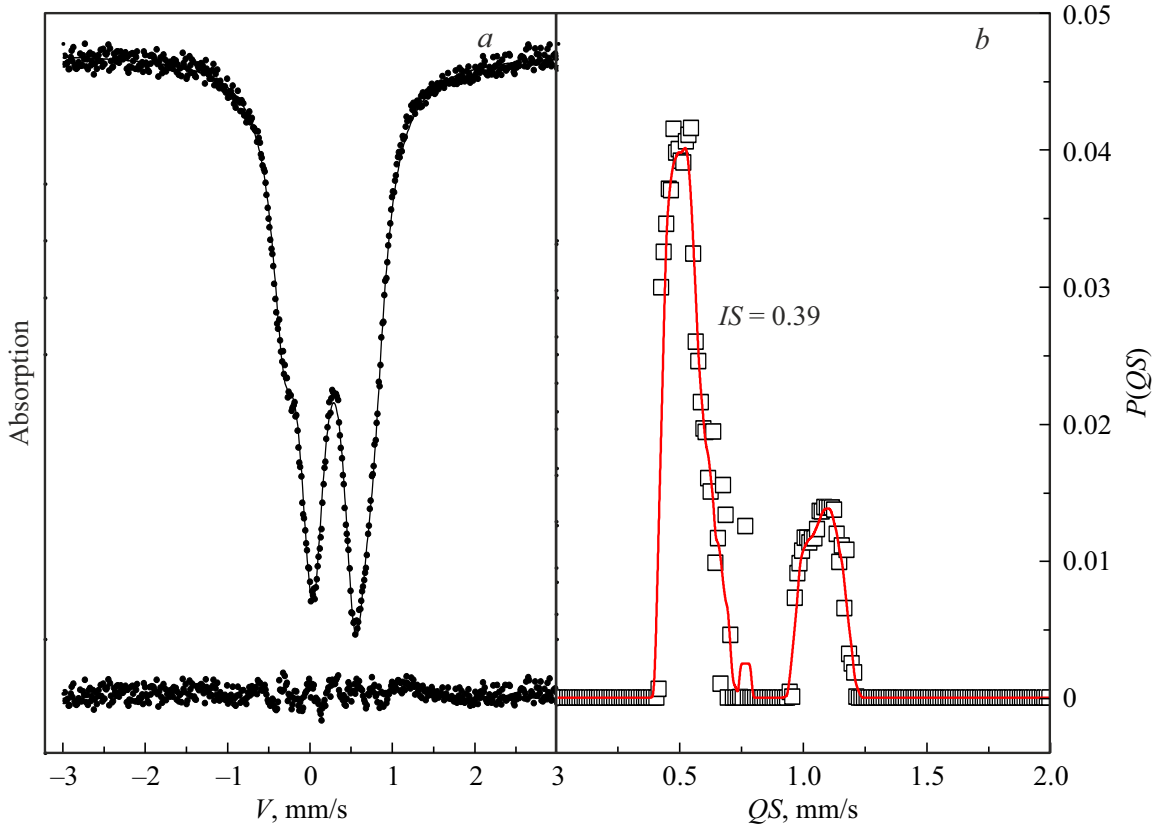

Figure 3. *a*) — Room-temperature Mössbauer spectrum of $NaMnFe_2V_3O_{12}$. Its parameters are listed in Table 4. The lower curve represents the difference between the experimental and calculated spectra. *b*) — Distribution of quadrupolar splittings in the experimental spectrum.

Table 4. Mössbauer parameters of vanadate $NaMnFe_2V_3O_{12}$: *IS* — isomeric chemical shift relative to α-Fe, *QS* — quadrupolar splitting, *W* — absorption line width, and *A* — fractional occupancy of the non-equivalent iron site

Compound	*IS*, mm/s ±0.01	*QS*, mm/s ±0.02	*W*, mm/s ±0.02	*A*, ±0.05	Site
$NaMnFe_2V_3O_{12}$	0.39	0.52	0.38	0.73	$Fe^{3+}(6)$
	0.33	1.08	0.33	0.27	$Fe^{3+}(5)$

assumption is also supported by certain features of temperature dependences of the resonance field: this field of signal *2* decreases with decreasing temperature, whereas the resonance field of signal *1* is virtually independent of temperature.

3.3. Results of static magnetic measurements of polyvanadate $NaMnFe_2V_3O_{12}$

Figure 6 shows the temperature dependences of magnetic moment m (a) and inverse magnetic susceptibility χ^{-1} (b) measured in magnetic field $H = 500$ Oe for vanadate $NaMnFe_2V_3O_{12}$.

It was found that the variation of inverse magnetic susceptibility with temperature $\chi^{-1}(T)$ follows the Curie–Weiss law in the high-temperature region $(T > 50\,\mathrm{K})$. Asymptotic Néel temperature $\theta = -147\,\mathrm{K}$ is indicative of predominantly antiferromagnetic exchange interactions in the magnetic subsystem of $NaMnFe_2V_3O_{12}$ formed by mixed chains of magnetic iron Fe^{3+} and manganese Mn^{2+} cations with $3d^5$ electronic configurations (electron spin $S = 5/2$ and orbital angular momentum $L = 0$).

The experimental molar value of effective magnetic moment $\mu_{\mathrm{eff(exp)}} = 9.9\,\mu_B$ is close to its calculated value $\mu_{\mathrm{eff(calc.)}} = 10.2\,\mu_B$ ($\mu^{\mathrm{Fe3+}}_{\mathrm{eff(calc)}} = 5.91\,\mu_B$ and $\mu^{\mathrm{Mn2+}}_{\mathrm{eff(calc)}} = 5.91\,\mu_B$).

Figure 7 shows the temperature dependences of magnetic moment $m(T)$ of the $NaMnFe_2V_3O_{12}$ compound measured in a magnetic field of 10 Oe for a sample cooled to a

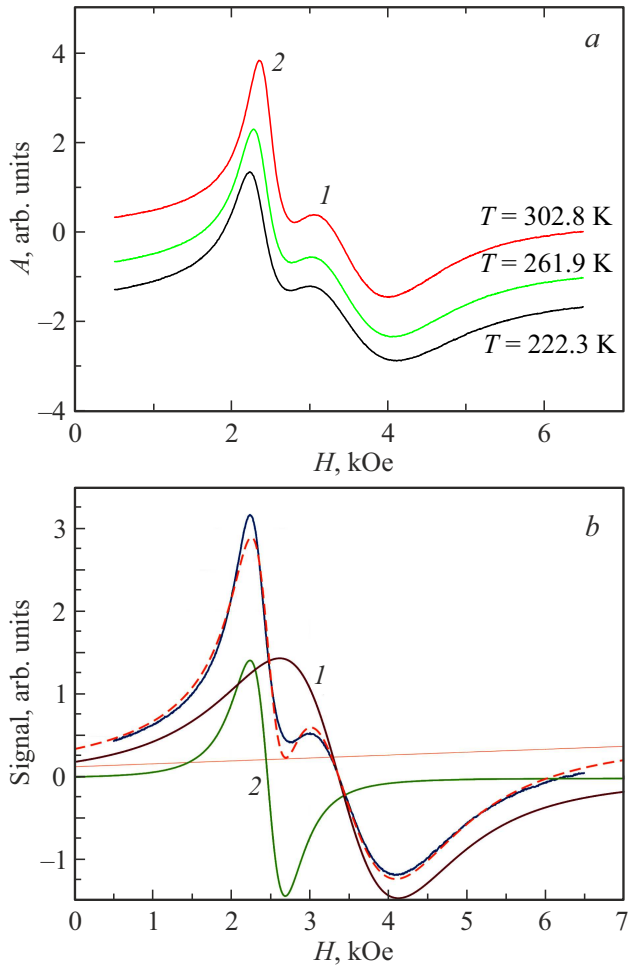

Figure 4. *a*) EPR spectrum of $NaMnFe_2V_3O_{12}$ at a frequency of 9 GHz and temperatures $T = 302.8$ K, 261.9 K, and 222.3 K. *b*) Result of fitting of the experimental EPR spectrum at $T = 302.8$ K with two Lorentzian curves (solid curve — experiment; dotted curve — fit).

temperature of 4.2 K in zero field (ZFC) and in magnetic field $H = 10$ Oe (FC). At temperature $T_F < 10.5$ K, the temperature variation of the magnetic moment depends on the thermal history of the sample (Figure 7), which is apparently induced by disorder in the spin system. The dependence of magnetic properties on the thermal history of the sample is characteristic of the spin glass magnetic state [14–16].

The level of magnetic frustrations estimated for the $NaMnFe_2V_3O_{12}$ compound as $f = |\theta|/T_F$ [17,18] (θ is the asymptotic Néel temperature and T_F is the critical temperature below which magnetic order is established) was high: $f \approx 14$ in magnetic field $H = 10$ Oe.

4. Conclusion

It may be noted that the results of a comprehensive study of the structural, static magnetic, and resonant properties of polyvanadate $NaMnFe_2V_3O_{12}$ allowed us to characterize a new compound obtained by solid-phase synthesis from Na_2CO_3, Fe_2O_3, $MnCO_3$, and V_2O_5 oxides at a temperature of 650 K and draw the following conclusions.

The crystal structure of $NaMnFe_2V_3O_{12}$ belongs to the trigonal system (space group $P1$) with lattice cell parameters $a = 6.7624(2)$ Å, $b = 8.2444(3)$ Å, $c = 9.8570(3)$,

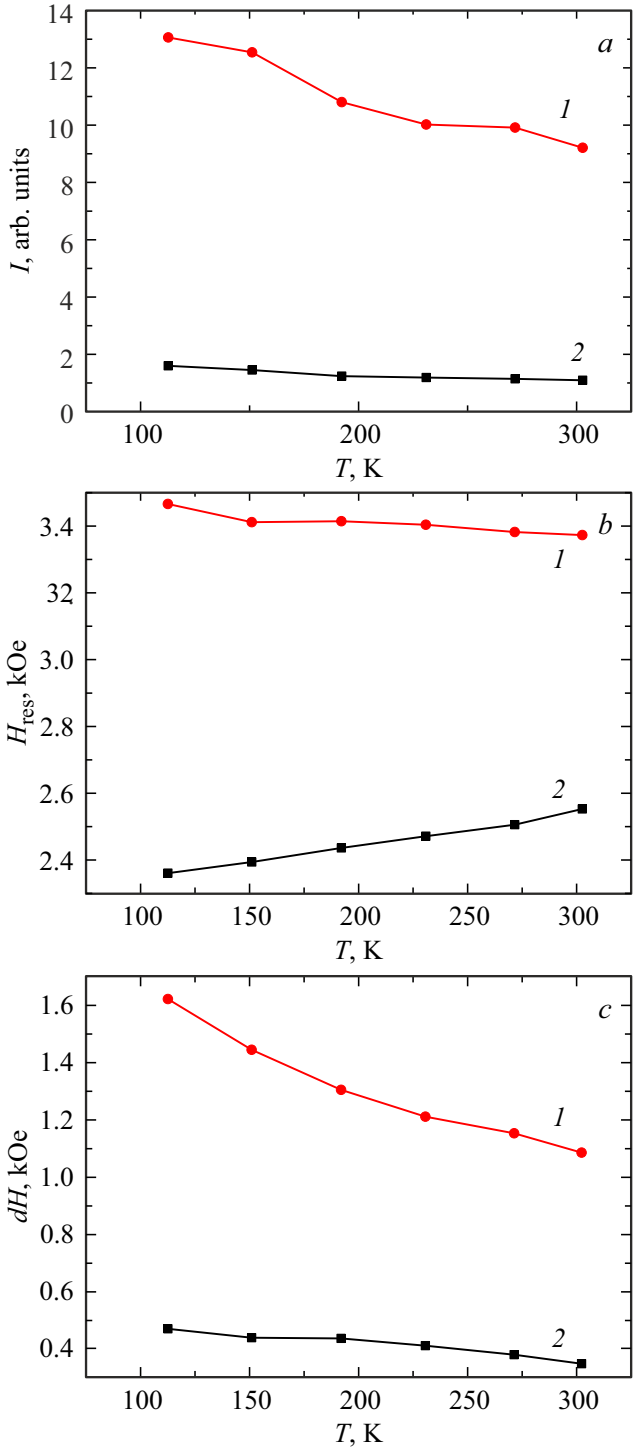

Figure 5. Temperature dependences of intensity$I$ (a), resonance field H_{res} (b), and line width dH (c) of the EPR signal at frequency $\nu = 9$ GHz in $NaMnFe_2V_3O_{12}$.

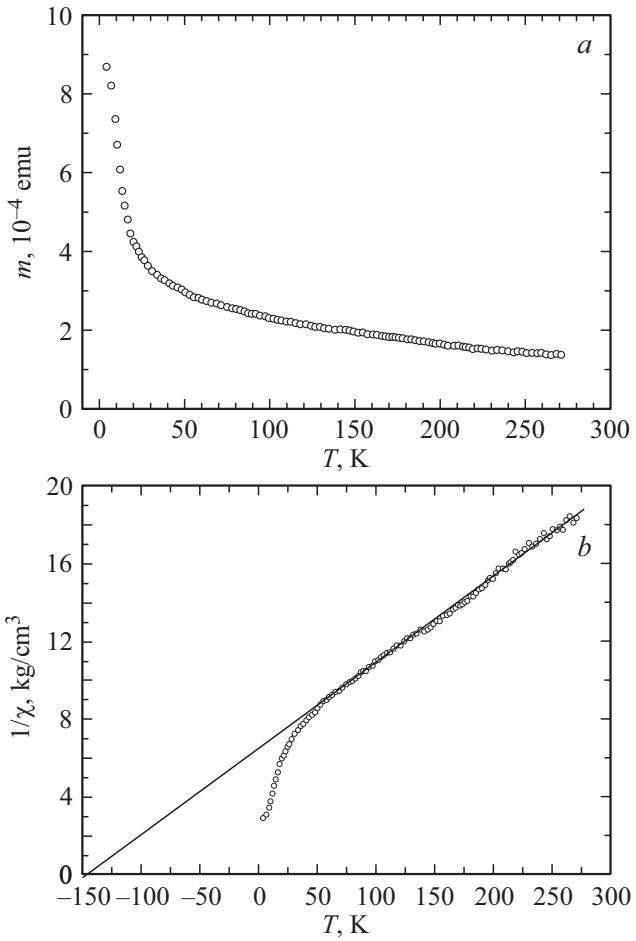

Figure 6. Temperature dependences of magnetic moment m (a) and inverse magnetic susceptibility χ^{-1} (b) in $NaMnFe_2(VO_4)_3$ measured in magnetic field $H = 500$ Oe; sample mass $m = 0.00508$ g. Asymptotic Néel temperature $\theta = -147$ K.

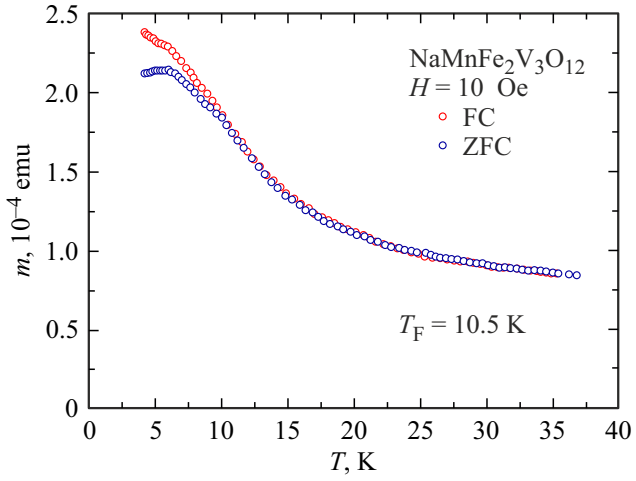

Figure 7. Temperature dependences of magnetic moment m under different sample cooling conditions (ZFC — zero-field cooling; FC — cooling in external magnetic field $H = 10$ Oe). Freezing temperature $T_F = 10.5$ K.

$\alpha = 105.935(2)°$, $\beta = 104.761(3)°$, $\gamma = 102.761(3)°$, and $V = 487.38(3)$ Å^3; the number of molecules in the lattice cell is $Z = 2$. The $NaMnFe_2V_3O_{12}$ structure cell contains six mixed sites occupied by Fe^{3+} and Mn^{2+} cations (two with bipyramidal oxygen environment and four with octahedral oxygen environment).

The examination of the distribution of iron cations in high-spin state $S = 5/2(d^5)$ revealed that the occupancy of octahedral sites is approximately three times higher than that of bipyramidal sites.

The high frustration index of competing magnetic interactions and the presence of atomic disorder in the sample due to a non-uniform distribution of iron cations over six non-equivalent crystallographic sites and their mixing with manganese cations suggest that a magnetic spin glass state is likely to be established at temperatures below 10.5 K.

Funding

This study was carried out as part of the state research assignment of the Kirensky Institute of Physics. The authors wish to thank the Krasnoyarsk Regional Research Equipment Sharing Center of the Federal Research Center „Krasnoyarsk Science Center of the Siberian Branch of the Russian Academy of Sciences“ for providing the equipment needed to examine the structural properties and measure the EPR characteristics.

Conflict of interest

The authors declare that they have no conflict of interest.

References

[1] A.A. Fotiev, B.V. Slobodin, M.Ya. Khodos. Vanadaty. Sostav, sintez, struktura, svoistva. Nauka, M. (1988). (in Russian).
[2] G. Zolnierkiewicz, N. Guskos, J. Typek, E.A. Anagnostakis, A. Blonska-Tabero, M. Bosacka. J. Alloys Compd. **471**, 28 (2009).
[3] T.V. Drokina, G.A. Petrakovskii, O.A. Bayukov, A.M. Vorotynov, D.A. Velikanov, M.S. Molokeev. Phys. Solid State **58**, 1981 (2016).
[4] A.V. Koshelev, K.V. Zakharov, L.V. Shvanskaya, A.A. Shakin, D.A. Chareev, S. Kamusella, H.-H. Klauss, K. Molla, B. Rahaman, T. Saha-Dasgupta, A.P. Pyatakov, O.S. Volkova, A.N. Vasiliev. Phys. Rev. Appl. **10**, 034008 (2018).
[5] A.A. Belik. Mater. Res. Bull. **34**, *12*, 1973 (1999).
[6] T.V. Drokina, G.A. Petrakovskii, O.A. Bayukov, M.S. Molokeev, A.M. Vorotynov, S.I. Popkov, D.A. Velikanov. Phys. Solid State **62**, 297 (2020).
[7] T.V. Drokina, D.A. Velikanov, O.A. Bayukov, M.S. Molokeev, G.A. Petrakovskii. Phys. Solid State **63**, 802 (2021).
[8] T.V. Drokina, O.A. Bayukov, D.A. Velikanov, A.L. Freidman, G.A. Petrakovsky. Phys. Solid State **65**, 255 (2023).
[9] T.V. Drokina, M.S. Molokeev, D.A. Velikanov, O.A. Bayukov, A.M. Vorotynov, A.L. Freidman, G.A. Petrakovsky. Phys. Solid State **65**, 1278 (2023).
[10] D.A. Velikanov. Inorg. Mater.: Appl. Res. **11**, 801 (2020). DOI: 10.1134/S2075113320040413.

[11] D.A. Velikanov. Magnitometr so sverkhprovodyashchim kvantovym interferometricheskim datchikom. RF Patent No. 2481591. Published on May 10, 2013, Byull. No. 13. (in Russian).
https://worldwide.espacenet.com/patent/search?q=RU2481591
[12] F.D. Martin, H. Müller-Buschbaum. Z. Naturforsch. B **50**, *1*, 51 (1995).
[13] Bruker AXS TOPAS V4: General profile and structure analysis software for powder diffraction data. — User's Manual. Bruker AXS, Karlsruhe (2008).
[14] I.Ya. Korenblit, E.F. Shender. Sov. Phys. Usp. **32**, 139 (1989).
[15] K. Binder, A.P. Yang. Rev. Mod. Phys. **58**, 801 (1986).
[16] J.A. Mydosh. Spin-Glasses: An Experimental Introduction. Taylor and Francis, N.Y. (1993).
[17] J.E. Greedan, A.P. Ramirez. Comments Condens. Matter Phys. **18**, *1*, 21 (1996).
[18] J.E. Greedan. J. Mater. Chem. **11**, 37 (2000).

Translated by D.Safin